Shoreline extraction using satellite imagery

Michalis Lipakis, Nektarios Chrysoulakis, Yiannis Kamarianakis

Shoreline change is considered to be one of the most dynamic processes in the coastal area. It has become important to map shoreline changes as an input data for coastal hazard assessment. In recent years, satellite remote sensing data has been used in shoreline extraction and mapping. The accuracy of image orthorectification, as well as the accuracy of image classification, are the most important factors affecting the accuracy of the extracted shoreline. In this study, the shoreline of the area of Georgioupolis was mapped for the years 1998 and 2005 using aerial imagery and Ikonos data, respectively. Ikonos data were orthorectified and a feature extraction technique was then used to extract the shoreline. This technique employed machine-learning algorithms which exploit both the spectral and spatial information of the image. Results were validated with *in situ* measurements using Differential GPS. The analysis showed that there have not been severe changes in the shoreline between 1998 and 2005, except in some locations where change was substantial.

Introduction

The coastal area is a highly dynamic environment with many physical processes, such as tidal flooding, sea level rise, land subsidence, and erosion-sedimentation. Those processes play an important role in shoreline change and development of the coastal landscape. Multi-year shoreline mapping is considered to be a valuable task for coastal monitoring and assessment. The shoreline is defined as the line of contact between land and a body of water. It is easy to define but difficult to capture, since the water level is always changing. Therefore, a problem exists in the mapping community because different public or private entities have compiled and published shoreline delineations that are based on different shoreline definitions. This has created confusion and uncertainty for those who use shoreline information daily for the sake of decision making, resource planning, emergency preparedness etc. In the USA for example, NOAA uses the tide-coordinated shoreline, which is the shoreline extracted from a specific tide water level. The MLLW (Mean Lower Low Water) and MHW (Mean High Water) are used in this way to map shorelines that can be geo-referenced. Both the MLLW and MHW are calculated from averages over a period of 18.6 lunar years (Li et al., 2001). In contrast, the U.S. Geological Survey (USGS) compiles shoreline data for the 1: 24.000 scale topographic base map series from digital orthophoto quadrangles created from photographs that are not tide coordinated, thereby making the shoreline a snapshot in time (Scott et al., 2003). It is therefore obvious that since shoreline has a dynamic nature, its definition, mapping and monitoring are complicated tasks.

Different approaches to shoreline mapping and change detection have been used in the past. Traditional shoreline mapping in small areas is carried out using conventional field surveying methods. The method used today by the American National Geodetic Survey to delineate the shoreline is analytical stereo photogrammetry using tide-coordinated aerial photography controlled by kinematic GPS techniques (Di et al., 2003). Land vehicle-based mobile mapping technology has been proposed to trace

water marks along a shoreline using GPS receivers and a beach vehicle. LiDAR depth data have also been used to map shorelines (Shaw and Allen, 1995; Li, 1997).
Automatic extraction of shoreline features from aerial photos has been investigated using neural networks and image processing techniques (Ryan et al., 1991). Photogrammetric techniques have been employed to map the tide-coordinated shoreline from the aerial images that are taken when the water level reaches the desired level. Aerial photographs taken at these water levels are more expensive to obtain than satellite imagery.
Besides aerial imagery, space-born radar and especially Synthetic Aperture Radar (SAR) have proven to be a valuable tool for coastal monitoring. SAR imagery has also been used to extract shorelines at various geographic locations (Erteza, 1998; Chen and Shyu, 1998; Trebossen et al., 2005; Wu and Lee, 2007). SAR is a very promising technology, especially for Europe since the European Space Agency (ESA) is recognized as a world leader in SAR missions (ERS1, ERS2, Envisat, GMES-Sentinel-1).
In recent years, optical satellite remote sensing data have been used in automatic or semi-automatic shoreline extraction and mapping. Braud and Feng (1998) evaluated threshold level slicing and multispectral image classification techniques for detection and delineation of the Louisiana shoreline from 30-meter resolution Landsat Thematic Mapper (TM) imagery. They found that thresholding TM Band 5 was the most reliable methodology. Frazier and Page (2000) quantitatively analysed the classification accuracy of water body detection and delineation from Landsat TM data in the Wagga region in Australia. Their experiments indicated that the density slicing of TM Band 5 achieved an overall accuracy of 96.9 percent, which is as successful as the 6-band maximum likelihood classification. Scott et al. (2003) proposed a semi-automated method for objectively interpreting and extracting the land-water interface, which has been devised and used successfully to generate multiple shoreline data for the test States of Louisiana and Delaware. This method was based on the application of Tasseled Cap transformation coefficients derived by the EROS Data Center for ETM+ data as described by Huang et al. (2002). The Tasseled Cap transformation was chosen over other methods primarily because of the objective and consistent manner in which it classifies pixels and because its use allowed the creation of other useful raster byproduct files. In operation, the Tasseled Cap transformation recombined spectral information of the 6 ETM+ bands into 3 principal view components through the use of coefficients derived by sampling known land cover spectral characteristics. Of the three principal view components created, i.e., Brightness, Greenness, and Wetness, the Wetness component is exploited to differentiate land from water. Zakariya et al. (2006) tried to detect shoreline changes for the Terengganu river mouth and related coastal area. Landsat data were used together with GIS capability to determine shoreline, sandy area and the changes that occur especially on sediment movement from 1996 to 2002. RGB to IHS imagery conversion analysis ISODATA (Iterative Self-Organizing Data Analysis) classification were employed. Liu and Jezek (2004), as well as Karantzalos and Argialas (2007) automated the extraction of coastline from satellite imagery by canny edge detection using digital number (DN) threshold.
Li et al. (2001) compared shorelines of the same area that were extracted using different techniques, evaluated their differences and discussed the causes of possible shoreline changes. The different shoreline products had been generated using different techniques: by digitising from aerial orthophotos, intersecting a digital water surface with a coastal terrain model and extracting from stereo satellite images. In addition, existing shorelines digitised from USGS maps and NOAA T-Sheets were included in their analysis.
With the development of remote sensing technology, satellites can capture high resolution imagery with the capability of producing stereo imagery. The new generation of very high spatial resolution satellite imaging systems, such as Ikonos and Quickbird, opens a new era of earth observation and digital mapping. They provide not only high-resolution and multi-spectral data, but also the capability for stereo mapping. Because of their high resolution and their short revisit rate (~3 days), Ikonos and Quickbird satellite images are very valuable for shoreline mapping and change detection, therefore their data have been used in several past studies. Wang et al. (2003) investigated a novel approach for automatic extraction of shoreline from Ikonos images using a mean shift segmentation algorithm. Di et al. (2003) investigated a novel approach for automatic extraction of shorelines from Ikonos imagery:

4m and 1m resolution Ikonos images along the Lake Erie shore were used. In the first step the images were segmented into homogeneous regions by mean shift segmentation. Then, the major water body was identified and an initial shoreline was generated. The final shoreline was obtained by local refinement within the boundaries of the candidate regions adjacent to the initial shoreline. Li et al. (2003) used Ikonos stereo imagery in shoreline extraction. They presented the results of an experiment in which they attempted to improve Ikonos Rational Functions (RF) for a better ground accuracy and to employ the improved RF for 3-D shoreline extraction using 1-meter panchromatic stereo images in a Lake Erie coastal area. In this method, a 2D shoreline is extracted by manual digitising on one Ikonos image; then corresponding shoreline points on the other image of the stereo-pair are automatically extracted by image matching. The 3D shoreline is computed using photogrammetric triangulation. Chalabi et al. (2006) had used pixel-based segmentation on Ikonos image using DN threshold. The partition of the land and sea boundary was done using pseudo-colour which exhibits a strong contrast between land and water features.

Shoreline change is considered to be one of the most dynamic processes in coastal area. It has become important to map the shoreline change as an input data for coastal hazard assessment. There are many change detection techniques currently in use including visual interpretation, spectral-value-based technique (differencing, image regression, DN value analysis), multi-data composites, and change vector analysis. Visual interpretation of multi-temporal images for coastal monitoring was presented by Mazian et al. (1989) and Elkoushy and Tolba (2004). Bagli and Soille (2003) analysed DN value using slicing operation for change monitoring. In addition, Whithe and El Asmar (1999) introduced an algorithm function and DN analysis to deviate the water from the land. The DN value analysis has also been applied on Landsat images, e.g. by Frazier and Page (2000) and Marfai (2003). Fromard et al. (2004) identified coastal changes that took place over the last 50 years, and related them to natural processes of turnover and replenishment of mangrove forests. They used a combination of remote sensing techniques (aerial photographs and SPOT satellite images) and field surveys in the area of the Sinnamary Estuary, French Guiana. Mills et al. (2005) introduced the integration of the geomatics techniques to form accurate representations of the coastline. A highly accurate Digital Elevation Model (DEM), created using kinematics GPS, was used as control to orientate surfaces derived from the relative orientation stage of photogrammetry processing. Mostafa and Soussa (2006) have applied GIS and remote sensing technique to monitor the lake of Nasser including the shoreline dynamics. Three satellite Landsat images for Nasser Lake were available in a time series (1984, 1996, and 2001). Topography map of scale 1: 50.000, that is suitable to the resolution of Landsat images, was used for developing DEM. Chalabi et al. (2006) assessed multi-data sources for monitoring shoreline in Kuala Terengganu, Malaysia using Ikonos and aerial photographs. Results of time series data were combined to each other showing spatial change of shoreline. Marfai et al. (2007) illustrated the shoreline dynamics in a coastal area of Se marang - Indonesia using multisource spatial data. In spite of the technique and approach to shoreline monitoring and delineation, no single method has been implemented that is free from major disadvantages.

Therefore, shorelines of the same area may be extracted at different times using satellite data and represent changes that appeared in difference periods that are illustrated as differences among them. There are two possible interpretations of the shoreline differences. One is that the shoreline indeed changed in the real world. The other possibility is that the differences are introduced by shoreline mapping errors. The accuracy of the shoreline derived from 1 meter Ikonos imagery should be about 2m - 4m (Zhou and Li 2000; Li et al., 2001, Grodecki and Dial, 2003), considering the fact that the accuracy of 3D ground control points (GCPs) reaches 2m – 3 m, with GCPs and the accuracy of identifying and locating conjugate shoreline points is about 1.5 pixels (1m - 2m). An optimistic estimation of the shoreline accuracy derived from the 4-meter Ikonos images in this specific case is about 8.5m (Li et al., 2001).

In most of the aforementioned methods, the shoreline extraction using Ikonos orthoimagery is based on land cover classification to discriminate the pixels corresponding to water bodies from those corresponding to land. Following, the resulting thematic image is converted to vector coverage, usually

a polygon shapefile (ESRI, 2005) containing the polygons corresponding to each class. The shoreline is finally extracted from the polygon that corresponds to water by employing automatic or semi-automatic GIS procedures. Thus, the accuracy of the image orthorectification, as well as the accuracy of the image classification, is the most important factors affecting the accuracy of the extracted shoreline. The orthorectification accuracy was discussed above. Concerning classification accuracy, it depends on the spatial, spectral and radiometric resolution of the image, as well as on the classification method. Numerous studies have been carried out using satellite images to extract land cover types (Congalton, 1991; Ridd and Liu, 1998; Martin et al., 1988; Gong and Howarth, 1990; Chrysoulakis, 2003; Gallego, 2004). The majority of the past studies rely on remote sensing data to classify land cover types using either raw DN or calibrated radiance values. However, if very high spatial resolution data such as Ikonos images are used, the land cover classification of coastal areas may be problematic because of the heterogeneity and small spatial size of the surface materials, which leads to significant sub-pixel mixing (Foody, 2000; Kontoes et al., 2000). Therefore, the spatial context should be taken into account in image classification and object oriented algorithms should be used. Improvements in the accuracy of classification have been achieved using a variety of sophisticated approaches including the use of neural networks (Berberoglu et al., 2000), fuzzy logic (Bastin, 1997; Zang and Foody 1998;), texture analysis (Stuckens et al., 2000), machine learning (VLS, 2007) and incorporation of ancillary spatial data in the classification scheme (Harris and Ventura, 1995; Vogelmann et al., 1998, Stefanov et al., 2001).

Methodology

The Ikonos satellite provides global, accurate, high-resolution imagery for mapping, monitoring, and development. The panchromatic sensor with 82cm resolution and an 11.3km wide swath at nadir provides high resolution, intelligence-quality imagery. The multispectral sensor, simultaneously collecting blue, green, red, and near infrared bands with 3.28m resolution at nadir, provides natural-colour imagery for visual interpretation and colour-infrared imagery for remote sensing applications. Combining the multispectral imagery with the high resolution panchromatic results in 1-meter colour images (pan-sharpen product), which can be orthorectified afterwards. The orthorectification is needed to eliminate the geometric distortions, which will be explained below, so that image features have correct planimetric coordinates. Quantitative estimations such as shoreline detection are performed using orthorectified images.

Apart from the different techniques that can be applied for shoreline extraction and monitoring from high resolution satellite images, the processing chain consists of the following basic steps:

- acquisition of images and pre-processing;
- acquisition of the ground Control Points (GCPs) with image coordinates and map coordinates;
- computation of the unknown parameters of the mathematical functions used for the geometric correction model;
- image orthorectification using an appropriate DEM;
- automatic, semi-automatic or manual shoreline extraction from the orthorectified imagery;
- monitoring of shoreline changes by repeating the above steps at predefined time periods and comparing the relative positions of the extracted shorelines.

Thus, before the application of any algorithm for automatic extraction of shoreline from multispectral satellite images, these images should be othorectified to take into account the geometric distortions during image acquisition, as well as the effect of topography. Each image acquisition system produces unique geometric distortions in its raw images and consequently the geometry of these images does not correspond to the terrain or of course to a specific map projection. Obviously, the geometric distortions vary considerably with different factors such as the platform, the sensor and also the total field of view. However, as it has been described by Toutin (2004), it is possible to make general categorisations of these distortions. The sources of distortion can be grouped into two broad categories: the observer or the acquisition system (platform, imaging sensor and other measuring instruments, such as gyroscope, stellar sensors, etc.) and the observed (atmosphere and Earth). In addition to these distortions, the deformations related to the map projection have to be taken into account because

the terrain and most GIS end-user applications are generally represented and performed respectively in a topographic space and not in the geoid or a referenced ellipsoid. Most of these geometric distortions are predictable or systematic and generally well understood. Some of these distortions, especially those related to the instrumentation, are generally corrected at ground receiving stations or by image vendors. Others, for example those related to the atmosphere, are not taken into account and corrected because they are specific to each acquisition time and location and information on the atmosphere is rarely available. The remaining geometric distortions require models and mathematical functions to perform geometric corrections of imagery: either through 2D/3D empirical models (such as 2D/3D polynomial or 3D RF) or with rigorous 2D/3D physical and deterministic models. With 2D/3D physical models, which reflect the physical reality of the viewing geometry (platform, sensor, Earth and sometimes map projection), geometric correction can be performed step-by-step with a mathematical function for each distortion/deformation, or simultaneously with a combined mathematical function.

2D/3D physical functions used to perform the geometric correction differ, depending on the sensor, the platform and its image acquisition geometry (Toutin, 2004):

- instantaneous acquisition systems, such as photogrammetric cameras, Metric Camera or Large Format Camera;
- rotating or oscillating scanning mirrors, such as Landsat-MSS, TM and ETM+;
- push-broom scanners, such as SPOT-HRV, IRS-1C/D, Ikonos and Quickbird; and
- SAR sensors, such as JERS, ERS-1/2, RADARSAT-1/2 and Envisat.

Whatever the geometric model used, even with the RF some GCPs have to be acquired to compute/refine the parameters of the mathematical functions in order to obtain a cartographic standard accuracy. Generally, an iterative least-square adjustment process is applied when more GCPs than the minimum number required by the model (as a function of unknown parameters) are used. The number of GCPs is a function of different conditions: the method of collection, sensor type and resolution, image spacing, geometric model, study site, physical environment, GCP definition and accuracy and the final expected accuracy. The aerial triangulation method has been developed and applied with different optical and radar satellite data using 3D physical models (Toutin, 2003a, b), as well as with Ikonos data using 3D RF models (Fraser et al., 2002a, b). All model parameters of each image/strip are determined by a common least-squares adjustment so that the individual models are properly tied in and an entire block is optimally oriented in relation to the GCPs.

As it has been already motioned, shoreline extraction needs orthorectified images. To rectify the original image into a map image, there are two processing operations:

- a geometric operation to compute the cell coordinates in the original image for each map image cell, eliminating the geometric distortions as previously explained; and
- a radiometric operation to compute the intensity value or DN of the map image cell as a function of the intensity values of original image cells that surround the previously-computed position of the map image cell.

The geometric operation requires the observation equations of the geometric model with the previously computed unknowns, and sometimes elevation information. The 3D models take into account elevation distortion and DEMs is thus needed to create precise orthorectified images. DEMs impact on the orthorectification process, both in terms of elevation accuracy for the positioning accuracy and of grid spacing for the level of details. This last aspect is more important with high-resolution images because a poor grid spacing when compared to the image spacing could generate artefacts for linear features such as shorelines. For any map coordinates (x, y), with the z elevation extracted from a DEM when 3D models are used, the original image coordinates (column and line) are computed from the two resolved equations of the model. However, the computed image coordinates of the map image coordinates will not directly overlay in the original image; in other words, the column and line computed values will rarely, if ever, be integer values. Since the computed coordinate values in the original image are not integers, one must compute the DN to be assigned to the map image cell. In order to do this, the radiometric operation uses a resampling kernel applied to original image cells: either the DN

of the closest cell (called nearest neighbour resampling) or a specific interpolation or deconvolution algorithm using the DNs of surrounding cells (Toutin, 2004).

In order to accurately create or extract geographic information from raw Ikonos imagery, the Image Geometry Model (IGM) must accompany the imagery. The IGM consists of several metadata files which contain RPCs (rational polynomial coefficients). The RPCs are a series of coefficients that describe the relationship between the image as it existed when captured and the Earth's surface. Although they do not describe sensor parameters explicitly, RFs are simple to implement and perform transformations very rapidly. With the availability of RPCs, the Ikonos interior and exterior orientations are very accurate. Therefore Ikonos imagery can be orthorectified if the IGM, an accurate DEM and some GCPs are available by employing any photogrametric software such as Orthoengine (PCI, 2003) or Leica Photogrammetry Suite (Leica, 2005).

The next step for shoreline extraction is the water-land separation; therefore the orthorectified image should be classified or a polygon corresponding to water (or land) area should be extracted. Taking into account the aforementioned land cover mapping constraints for very high spatial resolution satellite data, a machine learning classifier approach seems the best solution for Ikonos multispectral image classification. This type of classifier uses an inductive learning algorithm to generate production rules from training data. As with a neural network, there are several advantages to using a machine-learning approach. Since ancillary data layers may be used to help improve discrimination between classes, fewer field samples are generally required for training. This machine learning model is non-parametric and does not require normally-distributed data or independence of attributes. It can also recognize nonlinear patterns in the input data that are too complex for conventional statistical analyses or too subtle to be noticed by an analyst. Feature Analyst software (VLS, 2007) was selected for shoreline extraction from Ikonos imagery, since it employs machine-learning techniques which have the potential to exploit both the spectral and spatial information of the image. It provides a paradigm shift to automated feature extraction since it: (a) utilises spectral, spatial, temporal, and ancillary information to model the feature extraction process, (b) provides the ability to remove clutter, (c) incorporates advanced machine learning techniques to provide unparalleled levels of accuracy, and (d) provides an exceedingly simple interface for feature extraction. It works by taking a small and simple set of training examples, learns from the examples, and classifies the remainder of the image. When classifying the contents of imagery, there are only a few attributes accessible to human interpreters. For any single set of imagery these are: Shape, Size, Colour, Texture, Pattern, Shadow, and Association. Traditional image processing techniques incorporate only colour (spectral signature) and perhaps texture or pattern into an involved expert workflow process. The shoreline extraction steps using Feature Analyst are shown in Figure 1.

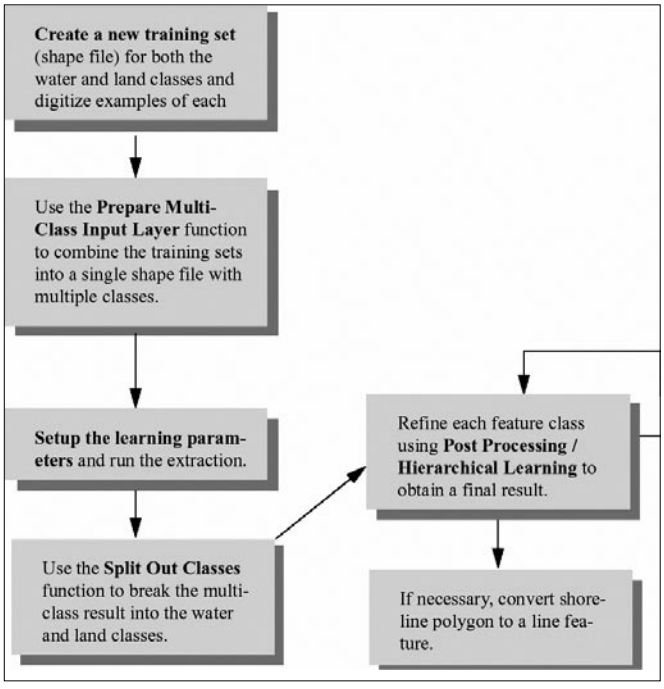

Figure 1 - Shoreline extraction work flow (adapted from VLS, 2007).

Case Study: Shoreline extraction in the area of Georgioupolis, Crete

The Shoreline extraction for the area of Georgioupolis was performed for the years 1998 and 2005 using aerial imagery and Ikonos data, respectively. The results validated with *in situ* measurements with Differential GPS (DGPS) provided by OANAK. The Hellenic Geodetic Reference System of 1987 (EGSA87) was used in all cases.

Shoreline extraction using an aerial image acquired in 1998

An orthorectified aerial image and a DEM of the broader area of Georgioupolis were available to OANAK as past project products. The aerial image has the spatial resolution of 1m, whereas its positional accuracy was better than 2 m (RMSExy < 2 m). It is shown in Figure 2, where the road network (produced by DGPS measurements) of the area has been superimposed (red lines). Feature Analyst was employed to classify the aerial orthoimage into 2 classes: land and water. The extraction of the shoreline was afterwards straightforward from the polygon corresponding to water class, using the ArcGIS software (ESRI, 2005). The latter will be also applied to Ikonos image, so it will be described in more detail below. The 1998 shoreline as extracted from the aerial image is also shown in Figure 2 (yellow line).

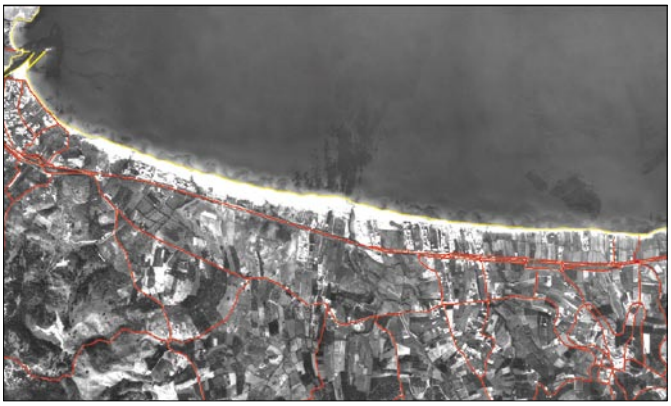

Figure 2 - Orthorectified aerial image acquired in 1998. The road network (red) and the extracted shoreline (yellow) have been superimposed.

Shoreline extraction using an Ikonos image acquired in 2005

The 2005 shoreline was extracted from an Ikonos multispectral image. ERDAS Imagine (Leica, 2005) was used to pre-process the image; LPS (Leica, 2005) was used to orthorectify the image; Feature Analyst (VLS, 2007) was used to extract the shoreline and ArcGIS (ESRI, 2005) was used to fine-tune the extracted shoreline. The processing chain included the following steps:

Step 1: Acquisition of images and pre-processing.

A panchromatic (PAN) and a four band (R, G, B, NIR) multispectral Ikonos image together with IGM and RPCs was provided by the image vendor as Raw Geo Product. The four channels are shown in Figure 3. ERDAS Imagine was used to merge the panchromatic and the multispectral images to provide a four-band pan-sharpen product with spatial resolution of 1m. The Wavelet Resolution Merge function (Leica, 2005) was used. The resulting pan-sharpen product is shown in Figure 4 as a pseudocolour composition RGB: 4-3-2.

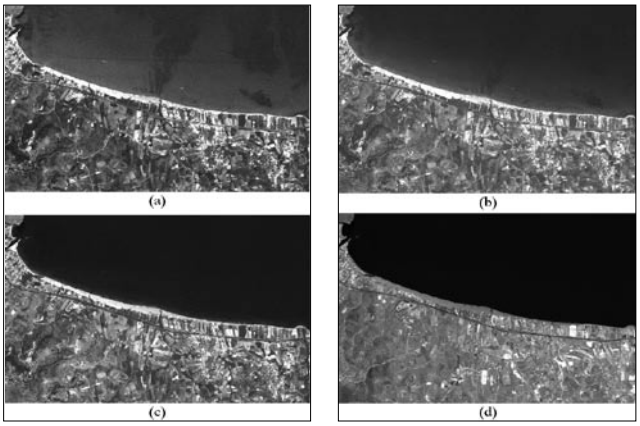

Figure 3 - Ikonos spectral channels of the 2005 acquisition over the area of Georgioupolis: a) blue band; b) green band; c) red band; d) near infrared band. The strong absorption of water in the near infrared band is obvious in d), therefore this band is the most useful for the discrimination between land and water.

Step 2: Acquisition of GCPs.
A field campaign was organized by OANAK and 15 GCP's were selected using a differential GPS. The location of these points (circles) superimposed to the road network of the study area is shown in Figure 5. Their positional accuracy was better than 1m (RMSExy < 1m). Several other GCPs were randomly selected to be used for validation of the orthorectification procedure.

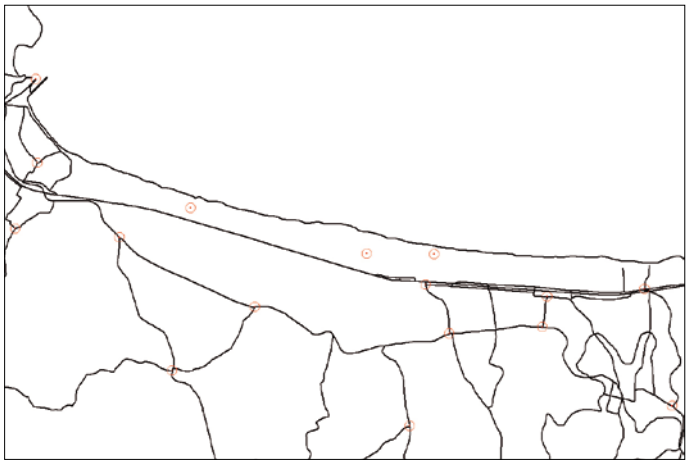

Figure 5 - Location of the measured GCPs superimposed to the road network of the study area.

Step 3: Computation of the unknown parameters of the mathematical functions used for the geometric correction model.
The interior and exterior orientations were automatically computed using LPS since the IGM and the GCP's were available. The aerial triangulation procedure (Leica, 2005) was followed. This procedure eliminated the geometric errors which have been previously discussed, except for the effect of topography. This effect was taken into account by using a DEM of the study area available at OANAK's. This DEM had been produced photogrammetrically using a stereo-pair of aerial images from the 1998 campaign. The vertical accuracy of the DEM was better than 1m (RMSEz < 1m). The DEM with the road network of the area superimposed is shown in Figure 6.

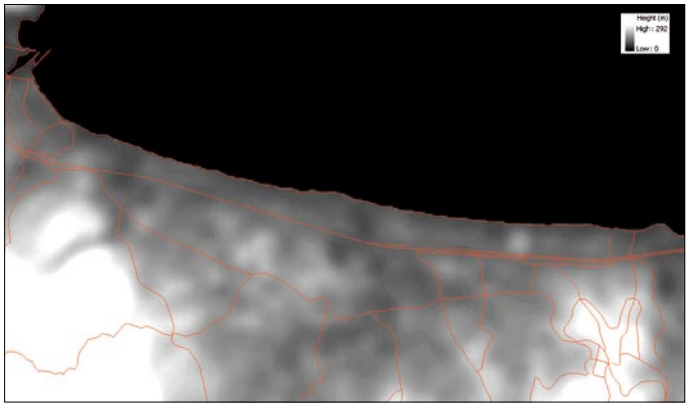

Figure 6 - The photogrammetrically derived DEM with the road network and the shoreline extracted from the aerial image superimposed.

Step 4: Orthorectification of images.
Since an accurate DEM was available and the aerial triangulation parameters were computed by LPS, the orthorectification procedure was also straightforward as a geometric and a radiometric operation,

as it has been already described. The orthorectification result is shown in Figure 7 as a pseudocolour composition RGB: 3-2-1, with the road network of the area (red lines) and the shoreline extracted from the aerial image (yellow line) superimposed. The spatial resolution of the othorectified image is 1m, whereas its positional accuracy is better than 2m (RMSExy < 2m), therefore, as it has been explained, the expected accuracy of the shoreline to be extracted is around 4m.

Figure 7 - Pseudocolour composition RGB: 3-2-1 of the orthorectified Ikonos pan-sharpened image with the road network (red lines) and the shoreline extracted from the aerial image (yellow line) superimposed. Differences in shoreline between 1998 and 2005 are obvious.

Step 5: Semi-automatic shoreline extraction using Feature Analyst.
The extraction of the shoreline using Feature Analyst is a semi-automatic procedure, as shown in Figure 1, involving:

- the creation of a new set containing two training classes;
- the preparation of a multi-class input layer;
- the setup of the learning parameters and the execution of the algorithm;
- the splitting of the two classes into a final polygon;
- the post processing, for smoothing of the result polygon;
- the conversion of the polygon into a line.

The first action is to create the training set of polygons. This is the most important action, because the quality of the results is dependant on the quality of the training sets. The training set will consist of two classes, one that corresponds to water elements and another one that corresponds to land elements. At this point, these two classes are indicated as two separate sets of polygons and then combined into a multi-class input layer. Creating the water set of polygons, includes a number of trials, to finally deicide and conclude to the most representative set. The result of these trials is a set of four polygons, three of which are located at the edge of the water mass, extending through the inshore, as shown in Figure 8 (purple). The same procedure is followed to decide about the land set. The result is a corresponding set of six polygons (blue).

Figure 8 - Pseudocolour composition RGB: 3-2-1 of the orthorectified Ikonos pan-sharpened image with the water (purple) and land (blue) training polygons superimposed.

In order to run a multi-class extraction, the two different classes of water and land have to be combined into a single, multi-class layer. There is a built-in function of Feature Analyst for this. The produced two-class layer is the input of the algorithm.
Having the input, the next action is to set the algorithm's parameters (VLS, 2007). All four image bands are about to be included and the image resolution is set to 1m. The spectral information is derived from this multispectral image, whereas the spatial context for each pixel is taken into account by adjusting the input representation of the classification algorithm. The input representation, that determines how each pixel is looked at in relation to its neighbours, is set to "Manhattan" representation (VLS, 2007). Manhattan is a pre-defined input pattern, used mainly for water mass and land cover features, like oceans, lakes, floods, wetland, impermeable surfaces, etc. The pattern width is set to 5. This means that considering that the "decision pixel" (red in Figure 9) is in the centre of a 5×5 grid, according to the Manhattan input representation, the algorithm will take into account 13 pixels (blue in Figure 9), located as shown in Figure 9. Computing 13 pixels of each band, there is a total of 52 pixels that will be computed to make a decision for a single pixel. The minimum aggregate area is set to 500 pixels. That is to maintain relative feature characteristics, while trying to find a large area.

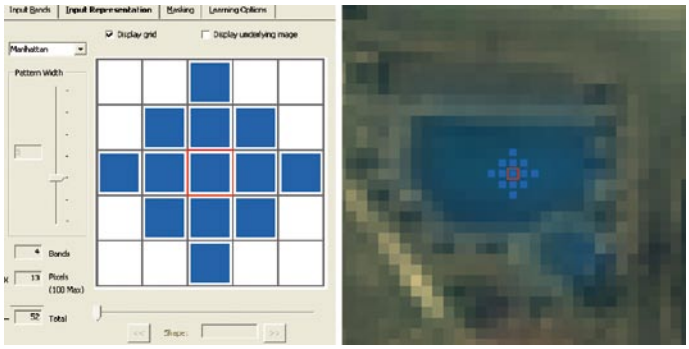

Figure 9 - The 'Manhattan' input representation that is used, with pattern width set to 5.

The classification result is shown in Figure 10. It is again a multi-class layer, which needs to be split. Although the border of both result classes is the same line (the shoreline), the water class is chosen for the extraction. The built-in function in Feature Analyst that splits out classes was used to split the classes and keep only the water class as a separate set. Since only one polygon has been left its border was smoothed in order to extract the shoreline. The "Bezier Smooth Algorithm" (VLS, 2007) was used, with the following parameters: the number of vertices to each side set to 2 and the maximum distance each vertex is allowed to move set to 3m. The result of the smoothed polygon is shown in Figure 11.

Figure 10 - The land – water classification result: a two class result corresponding to the two-class input. Both spectral and spatial information have been taken into account.

Figure 11 - The extracted – smoothed polygon corresponding to water.

Finally, the border of the water polygon was automatically extracted and converted to a line shapefile following a standard GIS procedure (VLS, 2007; ESRI, 2005). This line shapefile is the final result of the shoreline extraction procedure as it is shown in Figure 12, where the extracted shoreline has been superimposed on the orthorectified Ikonos image.

Figure 12 - Pseudocoloured composition RGB: 3-2-1 of the orthorectified Ikonos image with the extracted shoreline (yellow line) superimposed.

Step 6: Comparisons - Validation.
The produced shorelines (1998 Shoreline, and 2005 Shoreline) were compared and a Root Mean Square Error (RMSE) was computed to reflect the shoreline change during this 7 years period. RMSE is a global measure, thus the maximum change was highlighted and it is presented below. The RMSE was used as a quantitative evaluation of the extracted shorelines accuracy. RMSE encompasses both systematic and random errors and is defined as [1]:

$$RMSE = \sqrt{\frac{1}{n}\sum_{i=1}^{n} \delta s_i^2} \qquad [1]$$

Where:
δsi = minimum distance of the two lines at a pre-defined location i (x, y),
n = number of measuring locations in this study.

Finally, both the image-derived shorelines were compared with an *in situ* derived shoreline which was produced by OANAK with the use of differential GPS. The three lines are shown in Figure 13, where a part of the study area has been extracted (scale 1: 2.000): The *in situ* derived shoreline is presented in red, the 1998 Shoreline is presented in green and the 2005 Shoreline is presented in yellow. The RMSE calculated using the *in situ* line as baseline, as well as the RMSE between the extracted shorelines for 1998 and 2005, are shown in Table 1.

Figure 13 - Part of the study area as a pseudocolour composition RGB: 3-2-1 of the orthorectified Ikonos image (scale 1:2000). The in situ derived shoreline is shown in red, the 1998 Shoreline is shown in green, whereas the 2005 Shoreline is shown in yellow.

The analysis showed that there were not severe changes in shoreline between 1998 and 2005, except in some locations where the change was substantial. The most important change is shown in Figure 14, where a part of the study area around the river which is close to the town of Georgioupolis has been extracted (scale 1: 2.000): both lines have been superimposed on the Ikonos orthorectified image. The 1998 Shoreline is presented in green and the 2005 Shoreline is presented in yellow, as before. It is obvious from Figure 14 that the outfall of the river has been modified during this 7 year period. A shift of about 50m to the ESE direction can be observed in Figure 14.

Table 1 - RMSE between a) in situ and aerial image derived shoreline (1998); b) in situ and Ikonos derived shoreline (2005); c) aerial image and Ikonos derived shoreline.

Pair of Lines	RMSE (m)
In situ – 1998 Shoreline	3.01
In situ – 2005 Shoreline	5.65
1998 Shoreline– 2005 Shoreline	6.46

Figure 14 - Part of the study area as a pseudocolour composition RGB: 3-2-1 of the orthorectified Ikonos image (scale 1:2000). The 1998 Shoreline is shown in green and the 2005 Shoreline is shown in yellow. A shift of about 50m to the ESE direction of the river outflow is observed.

References

Bagli S. and Soille P. (2003) - *Morhological automatic extraction of Pan-European coastline from Landsat ETM+ images*. International Symposium on GIS and Computer Cartography for Coastal Zone Management. Genova, Italy.

Bastin L. (1997) *Comparison of fuzzy c-means classification, linear mixture modeling and MLC probabilities as tools for unmixing coarse pixels*. International Journal of Remote Sensing, 18: 3629 – 3648.

Berberoglu S., Lloyd C.D., Atkinson P.M. and Curran P.J. (2000) - *The integration of spectral and textural information using neural networks for land cover mapping in the Mediterranean*. Computers & Geosciences, 26: 385 – 396.

Braud D.H. and Feng W. (1998) - *Semi-automated construction of the Louisiana coastline digital land/water boundary using Landsat Thematic Mapper satellite imagery*. Department of Geography & Anthropology, Louisiana State University. Louisiana Applied Oil Spill Research and Development Program, OSRAPD Technical Report Series 97-002.

Chalabi A., Mohd-Lokman H., Mohd-Suffian I., Karamali K., Karthigeyan V. and Masita M (2006) - *Monitoring shoreline change using Ikonos image and aerial photographs: a case study of Kuala Terengganu area, Malaysia*. In: Proceedings of the ISPRS Mid-term Symposium Proceeding. Enschede, The Netherlands.

Chen L.C. and Shyu C.C. (1998) - *Automated Extraction of Shorelines from Optical and SAR Image*. In: Proceeding of Asian Conference on Remote Sensing (http://www.gisdevelopment. net/ aars/acrs/1998/ps3/ps3013a.asp).

Chrysoulakis N. (2003) - *Estimation of the all-wave urban surface radiation balance by use of ASTER multispectral imagery and in situ spatial data*. Journal of Geophysical Research, 108: 4582 (DOI:10.1029/2003JD003396).

Congalton R.G. (1991) - *A Review of Assessing the Accuracy of Classifications of Remotely Sensed Data*. Remote Sensing of Environment, 37: 35-46.

Di K., Wang J., Ma R. and Li R. (2003) - *Automatic shoreline extraction from high-resolution Ikonos satellite imagery*. In proceeding of the Annual ASPRS Conference. Anchorage, Alaska.

Elkoushy A.A. and Tolba R.A. (2004) - *Prediction of shoreline change by using satellite aerial imagery*. In: Proceeding of the XX ISPRS Congress. Istanbul, Turkey.

Erteza I.A. (1998) - *An automatic coastline detector for use with SAR images*. SANDIA Report SAND98-2102. Sandia National Laboratories, California.

ESRI (2005) - *ArcGIS 9. What is ArcGIS 9.1?* Environmental Systems Research Institute, California.

Foody G.M. (2000) - *Estimation of sub-pixel land cover composition in the presence of untrained classes*. Computers & Geosciences, 26: 469 – 478.

Fraser C.S., Hanley H.B. and Yamakawa T. (2002a) - *Three-dimensional geopositioning accuracy of Ikonos imagery*. Photogrammetric Record, 17: 465–479.

Fraser C.S., Baltsavias E. and Gruen A. (2002b) - *Processing of Ikonos imagery for sub-metre 3D positioning and building extraction*. ISPRS Journal of Photogrammetry and Remote Sensing, 56, 177–194.

Frazier P.S. and Page K.J. (2000) - *Water body detection and delineation with Landsat TM data*. Photogrammetric Engineering and Remote Sensing, 66: 147–167.

Fromard F., Vegaa C. and Proisy C. (2004) - *Half a century of dynamic coastal change affecting mangrove shorelines of French Guiana. A case study based on remote sensing data analyses and field surveys*. Marine Geology, 208: 265–280.

Gallego F.J. (2004) - *Remote sensing and land cover area estimation*. International Journal of Remote Sensing, 25: 3019-3047.

Gong P. and Howarth P.J. (1990) - *The use of structural information for improving land-cover classification accuracies at the rural – urban fringe*. Photogrammetric Engineering and Remote Sensing, 56: 67-73.

Grodecki J. and Dial G. (2003) - *Block adjustment of highresolution satellite images described by rational polynomials*. Photogrammetric Engineering and Remote Sensing, 69: 59-68.

Harris P.M. and Ventura S.J. (1995) - *The integration of geographic data with remotely sensed imagery to improve classification in an urban area*. Photogrammetric Engineering and Remote Sensing, 61: 993 – 998.

Huang C., Wylie B., Homer C., Yang L. and Zylstra G. (2002) - *Derivation of a tasseled cap transformation based on Landsat 7 ETM at-satellite reflectance*. International Journal of Remote Sensing, 23: 1741-1748.

Karantzalos K. and Argialas D. (2007) - *Automatic shoreline mapping from panchromatic satellite images*. In: Proceedings of 8th Pan-Hellenic Geographic Conference. Greek Geographical Society (in Greek).

Kontoes C.C., Raptis V., Lautner M. and Oberstadler R. (2000) - *The potential of kernel classification techniques for land use mapping in urban areas using 5 m-spatial resolution IRS-1C imagery*. International Journal of Remote Sensing, 21: 3145–3151.

Leica (2005) - *ERDAS Field Guide*. Leica Geosystems. Atlanta, Georgia, USA.

Li R., Di K. and Ma R. (2001) - *A Comparative Study of Shoreline Mapping Techniques*. In: Proceeding of the 4th International Symposium on Computer Mapping and GIS for Coastal Zone Management. Halifax, Nova Scotia, Canada.

Li R., Di K. and Ma R. (2003) - *3-D Shoreline Extraction from Ikonos Satellite Imagery*. Marine Geodesy, 26:107–115.

Li R. (1997) - *Mobile mapping: An emerging technology for spatial data acquisition*. Photogrammetric Engineering and Remote Sensing, 63: 1165-1169.

Liu H. and Jezek K.C. (2004) - *Automated extraction of coastline from satellite imagery by integrating canny edge detection and locally adaptive thresholding methods*. International Journal of Remote Sensing, 25: 937–958.

Marfai M.A., Almohammad H., Dey S., Susanto B. and King L. (2007) - *Coastal dynamic and shoreline mapping: multi-sourcesspatial data analysis in Semarang Indonesia*. Environ Monitoring and Assessment, DOI 10.1007/s10661-007-9929-2.

Marfai M.A. (2003) - *Monitoring of the coastal zone dynamics by means of multi-temporal Landsat TM*. In: Proceedings of the annual scientific meeting XII, Indonesian remote sensing society. Bandung.

Martin L.R.G., Howarth P.J. and Holder G. (1988) - *Multispectral classification of land use at the rural-urban fringe using SPOT data*. Canadian Journal of Remote Sensing, 14: 72 – 79.

Mazian H.I., Aziz I. and Abdullah A. (1989) - *Preliminary evaluation of photogrammetric-remote sensing approach in monitoring shoreline erosion*. In: Proccedings of the 10th Asian Conference on Remote Sensing Proceeding. Kuala Lumpur.

Mills J.P., Buckley S.J., Mitchell H.L., Clarke P.J. and Edwards S.J. (2005) - *A geomatics data integration technique for coastal change monitoring*. Earth Surface Processes and Landforms, 30: 651–664.

Mostafa M.M. and Soussa H.K. (2006) - *Monitoring of Lake Nasser using remote sensing and GIS techniques*. In: Proceedings of the ISPRS Mid-term Symposium. Enschede, The Netherlands.

PCI (2003) - *OrthoEngine User Guide*. PCI Geomatics. Ontario, Canada.

Ridd M.K. and Liu J. (1998) - *A comparison of four algorithms for change detection in an urban environment*. Remote Sensing of Environment, 63: 95 – 100.

Ryan T.W., Sementilli P.J., Yuen P. and Hunt B.R. (1991) - *Extraction of shoreline features by neural nets and image processing*. Photogrammetric Engineering and Remote Sensing, 57: 947-955.

Scott J.W., Moore L.R., Harris W.M. and Reed M.D. (2003) - *Using the Landsat 7 Enhanced Thematic Mapper Tasseled Cap Transformation to Extract Shoreline*. Open-File Report OF 03-272 U.S. Geological Survey.

Shaw B. and Allen J.R. (1995) - *Analysis of a dynamic shoreline at Sandy Hook, New Jersey, using a geographic information system*. In: Proceedings of ASPRS/ACSM. pp. 382-391.

Stefanov W.L., Ramseyc M.S. and Christensen P.R. (2001) - *Monitoring urban land cover change: An expert system approach to land cover classification of semiarid to arid urban centers*. Remote Sensing of Environment, 77: 173 – 185.

Stuckens J., Coppin P.R. and Bauer M.E. (2000) - *Integrating contextual information with per-pixel classification for improved land cover classification*. Remote Sensing of Environment, 71: 282 – 296.

Toutin Th. (2004) - *Review article: Geometric processing of remote sensing images: models, algorithms and methods*. International Journal of Remote Sensing, 25,1893–1924

Toutin Th. (2003a) - *Block bundle adjustment of Ikonos in-track images*. International Journal of Remote Sensing, 24: 851–857.

Toutin Th. (2003b) - *Error tracking in Ikonos geometric processing using a 3D parametric modelling*. Photogrammetric Engineering and Remote Sensing, 69: 43–51.

Trebossen H., Deffontaines B., Classeau N., Kouame J. and Rudant J.-P. (2005) - *Monitoring coastal evolution and associated littoral hazards of French Guiana shoreline with radar images*. Comptes Rendus Geosciences, 337: 1140-1153.

Vogelmann J.E., Sohl T. and Howard S.M. (1998) - *Regional characterization of land cover using multiple sources of data*. Photogrammetric Engineering and Remote Sensing, 64: 45 – 57.

VLS (2007) - *Feature Analyst Version 4.1 for Imagine*. Reference Manual. Visual Learning Systems Inc. Missoula, USA.

Wang K.D.J., Ma R. and Li R. (2003) - *Automatic shoreline extraction from high resolution Ikonos satellite imagery*. In: Proceedings of the ASPRS Annual Conference. Anchorage, Alaska.

Whithe K. and El Asmar H.M. (1999) - *Monitoring changing position of coastline using thematic mapper imagery, an example from the Nile Delta*. Geomorphology, 29: 93–105.

Wu T.D. and Lee M.T. (2007) - *Geological Lineament and Shoreline Detection in SAR Images*. Proceedings of IEEE Geosciences and Remote Sensing Symposium (IGARSS 2007). Barcelona, Spain.

Zakariya R., Rosnan Y., Saidin S.A., Yahaya M.H., Kasawani I. and Lokman H. (2006) - *Shoreline detection and changes for Terengganu river mouth from satellite imagery (Landsat 5 and Landsat 7)*. Journal of Sustainability Science and Management, 1: 47-57.

Zang J. and Foody G.M. (1998) - *A fuzzy classification of sub-urban land cover from remotely sensed imagery*. International Journal of Remote Sensing, 19: 2721 - 2738.

Zhou G. and Li R. (2000) - *Accuracy Evaluation of Ground Points from IKONOS High-Resolution Satellite Imagery*. Photogrammetric Engineering and Remote Sensing, 66: 1103-1112.